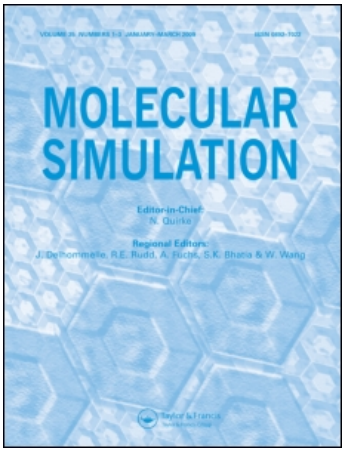

Molecular Simulation

Publication details, including instructions for authors and subscription information:
http://www.informaworld.com/smpp/title~content=t713644482

Ab initio and molecular dynamics studies of solid β-HMX: effects of hydrostatic pressure and high temperature

Hong-Ling Cui[ab]; Guang-Fu Ji[ac]; Ji-Jun Zhao[cd]; Feng Zhao[a]; Xiang-Rong Chen[b]; Qing-Ming Zhang[c]; Dong-Qing Wei[ce]

[a] National Key Laboratory of Shock Wave and Detonation Physics, Institute of Fluid Physics, Chinese Academy of Engineering Physics, Mianyang, P.R. China [b] Institute of Atomic and Molecular Physics, Sichuan University, Chengdu, P.R. China [c] State Key Laboratory of Explosion Science and Technology, Beijing Institute of Technology, Beijing, P.R. China [d] Laboratory of Materials Modification by Laser, Electron, and Ion Beams and College of Advanced Science and Technology, Dalian University of Technology, Dalian, P.R. China [e] College of Life Science and Biotechnology, Shanghai Jiaotong University, Shanghai, P.R. China

Online publication date: 16 August 2010

To cite this Article Cui, Hong-Ling , Ji, Guang-Fu , Zhao, Ji-Jun , Zhao, Feng , Chen, Xiang-Rong , Zhang, Qing-Ming and Wei, Dong-Qing(2010) '*Ab initio* and molecular dynamics studies of solid β-HMX: effects of hydrostatic pressure and high temperature', Molecular Simulation, 36: 9, 670 — 681

To link to this Article: DOI: 10.1080/08927021003720520

URL: http://dx.doi.org/10.1080/08927021003720520

Molecular Simulation
Vol. 36, No. 9, August 2010, 670–681

Taylor & Francis
Taylor & Francis Group

Ab initio and molecular dynamics studies of solid β-HMX: effects of hydrostatic pressure and high temperature

Hong-Ling Cui[ab], Guang-Fu Ji[ac]*, Ji-Jun Zhao[cd], Feng Zhao[a], Xiang-Rong Chen[b], Qing-Ming Zhang[c] and Dong-Qing Wei[ce]

[a]*National Key Laboratory of Shock Wave and Detonation Physics, Institute of Fluid Physics, Chinese Academy of Engineering Physics, Mianyang 621900, P.R. China;* [b]*Institute of Atomic and Molecular Physics, Sichuan University, Chengdu 610064, P.R. China;* [c]*State Key Laboratory of Explosion Science and Technology, Beijing Institute of Technology, Beijing 100081, P.R. China;* [d]*Laboratory of Materials Modification by Laser, Electron, and Ion Beams and College of Advanced Science and Technology, Dalian University of Technology, Dalian 116024, P.R. China;* [e]*College of Life Science and Biotechnology, Shanghai Jiaotong University, Shanghai 200240, P.R. China*

(*Received 28 October 2009; final version received 22 February 2010*)

Using first-principles density functional theory and classical molecular dynamics (MD), the structural, electronic and mechanical properties of the energetic material β-HMX have been studied. The crystal structure optimised by the local density approximation calculations compares reasonably with the experimental data. Electronic band structure and density of states indicate that β-HMX is an insulator with a band gap of 3.059 eV. The pressure effect on the crystal structure and physical properties has been investigated in the range of 0–40 GPa. The crystal structure and electronic properties change slightly as the pressure increases from 0 to 2.5 GPa; when the pressure is above 2.5 GPa, further increment of the pressure results in significant changes in crystal structure. There is a larger compression along the *b*-axis than along the *a*- and *c*-axes. Isothermal–isobaric MD simulations on β-HMX were performed in the temperature range of 5–400 K. Phase transition at 360 K, corresponding to a volume interrupt, was found. The computed thermal expansion coefficients show anisotropic behaviour with a slightly larger expansion along the *b*- and *c*-axes than along the *a*-axis. In the temperature range of 5–360 K, β-HMX possesses good plasticity and its stiffness decreases with increasing the temperature.

Keywords: density functional theory; molecular dynamics; hydrostatic pressure and high temperature; β-HMX

PACS: 71.15.Mb; 65.40.-b

1. Introduction

Highly energetic (HE) materials have played an important technological role as explosives, propellants and fuels for a long time. Solid energetic materials have broad applications in industrial and military fields; their structures and mechanical properties under extreme conditions are important diathesis for the usage. Moreover, understanding these properties is important for the safety and efficiency of the energetic materials. Thus, comprehensive investigation of the structure, stability and physical properties of HE materials under high pressure and/or high temperature is desirable. However, it is difficult to carry out experiments to investigate the stability of HE materials under extreme conditions. As an alternative, computer simulations have a remarkable advantage with their capability of being safe, effective and economic, which makes computer simulations become an important way to comprehend the properties of HE materials under extreme conditions.

Octahydro-1,3,5,7-tetranitro-1,3,5,7-tetrazocine (HMX) [1] is a very important and useful energetic material. It has been widely used as a secondary explosive and propellant in various high-performance explosives and propellants for its thermal stability and high detonation velocity since its production in 1952 [1,2]. It is known that HMX exhibits four different crystal structures, three pure crystallisation phases α, β and δ, and a hydrate phase γ [3]. At ambient conditions, the β-HMX phase is the most stable form [4]. From X-ray [5] and neutron diffraction [6], it was determined that the crystalline β-HMX phase has a monoclinic $P2_1/c$ structure, with two molecules per unit cell and 13 independent elastic coefficients. Cady and Smith [3] observed two phase transitions at high temperature, i.e. one is the β-to-α transition at 375–377 K and the other is the solid α-to-δ transformation at 433–437 K. Using diamond anvil cell, angle-resolved synchrotron X-ray diffraction and micro-Raman spectroscopy, Yoo and Cynn [7] obtained the pressure–volume relations and Raman spectra of unreacted β-HMX under both quasi-hydrostatic pressure up to 45 GPa and non-hydrostatic pressure up to 10 GPa. Their results showed that the high-pressure behaviour of β-HMX strongly depends on the stress. Two phase transitions were also observed, namely a conformational change at 12 GPa with no apparent volume change

*Corresponding author. Email: cyfjkf@caep.ac.cn

ISSN 0892-7022 print/ISSN 1029-0435 online

DOI: 10.1080/08927021003720520
http://www.informaworld.com

and a phase transformation along with a 4% volume discontinuity at 27 GPa [7]. Using synchrotron angle-dispersive X-ray diffraction techniques, Gump and Peiris [8] measured isothermal pressure–volume equations of state of β-HMX under temperatures of 303, 373 and 413 K with both hydrostatic and non-hydrostatic compressions. At all temperatures, HMX remained in the β phase up to 5.8 GPa. Using scattering from a variety of acoustic phonons, Stevens and Eckhardt [9] obtained a complete stiffness tensor of β-HMX and observed the ordering of stiffness constants, i.e. C_{11} (18.4 GPa) > C_{22} (14.4 GPa) > C_{33} (12.4 GPa).

On the theoretical side, Sewell [10] simulated hydrostatic compression of crystalline β-HMX within a pressure range of 0–7.5 GPa using the Monte Carlo method and the rigid molecule approximation. Sewell and Menikoff [11] used a high-level quantum chemistry-based intramolecular and intermolecular force field to investigate the elastic coefficients and derived the isotropic moduli of the three pure polymorphs of HMX at ambient temperature, and to compute the room-temperature isotherms with a pressure range from 0 to 10.6 GPa. The molecular structures, energetic stabilities and bulk moduli of α-, β- and δ-HMX were calculated by Lewis et al. [12] using first-principles electronic structure calculations. Byrd and Rice [13] reported the volume and lattice constants of β-HMX up to 8 GPa from *ab initio* calculations. Zhu et al. [14] reported the electronic and vibrational properties of four polymorphs of HMX using density functional theory (DFT) within the local density approximation (LDA); and the simulated results reproduced the order of their impact sensitivity as: β-HMX < γ-HMX < α-HMX < δ-HMX. Lu et al. [15] investigated the structural and vibrational properties of the β-HMX crystals under hydrostatic pressure using DFT with the generalised gradient approximation (GGA) and found that the N—N bond lengths were significantly reduced under compression. Zerilli and Kuklja [16] obtained the complete equation of state for the β-HMX molecular crystal from first-principles calculations within a temperature range from 0 to 400 K. Despite the above efforts, the intramolecular geometries and mechanical properties of the β-HMX crystal (especially at high pressures and high temperatures), which are important for understanding the stability, sensitivity and safety of these energetic molecular crystals, have not been explored theoretically.

In this work, we performed DFT calculations to simulate the β-HMX crystal under different pressures and carried out molecular dynamics (MD) simulations to study the structural and mechanical properties of β-HMX under different temperatures. The effects of pressure and temperature on the crystal structure, electronic and mechanical properties have been examined.

2. Computational methods

2.1 DFT calculation simulations

In this study, first-principles calculations were performed using DFT [17] with the Vanderbilt-type ultrasoft pseudopotentials [18] and a plane-wave basis. The self-consistent field calculation of the electron wave functions was conducted using a density-mixing scheme [19] and the geometry structures were fully relaxed using the Broyden–Fletcher–Goldfarb–Shannon method [20]. GGA with Perdew–Burke–Ernzerhof (PBE) parameterisation [21] was employed. All DFT calculations were carried out using the Cambridge serial total energy package program [22]. The cut-off energy for the plane-wave basis was set to 500 eV. Brillouin zone sampling was performed using the Monkhorst–Pack [23] scheme with a *k*-point grid of $4 \times 2 \times 3$, which was found to be enough for the solid β-HMX with only weak intermolecular interaction. The choices of the kinetic energy cut-off and the *k*-point grid have been tested to ensure the convergence of total energies to within 0.01%. During the geometry relaxation, the total energy of the system was converged to less than 1.0×10^{-6} eV, the residual force less than 0.002 eV/Å, the displacement of atoms less than 0.002 Å and the residual bulk stress less than 0.1 GPa. We adopted the experimental structure as the initial crystal structure for β-HMX, with $a = 6.54$ Å, $b = 11.05$ Å, $c = 8.70$ Å and $\beta = 124.3°$ [7]. Our DFT calculations included one unit cell with two molecules. Starting from the equilibrium zero-pressure structure, we gradually applied the hydrostatic pressure to the β-HMX crystal up to 40 GPa.

2.2 MD simulations

In this paper, the MD simulations were performed with the DISCOVER module of the commercial software Materials Studio [24]. The condensed-phase optimised molecular potentials for atomistic simulation studies (COMPASS) force field [25] was used with a cut-off distance of 10.5 Å. The MD simulations were carried out in the NPT ensemble with the Berendsen barostat method [26] and the Andersen thermostat method [27] to control the system at 0 GPa pressure and in the temperature range of 5–400 K, respectively. The simulation supercell contains 96 HMX molecules and 2688 atoms, corresponding to a box of $4 \times 4 \times 3$ unit cells for the β-HMX crystal. The initial crystal lattice and atomic position were taken from experimental data [7]. The initial temperature and pressure were set as 5 K and 0 GPa, respectively. At each temperature, the system was first relaxed for 1×10^5 time steps in the equilibration run, followed by a production run of 1×10^5 time steps. The data from the production run were collected for subsequent analysis. A fixed time step of 1 fs was used in all MD simulations. The long-range non-bond Coulombic and van der Waals (vdW)

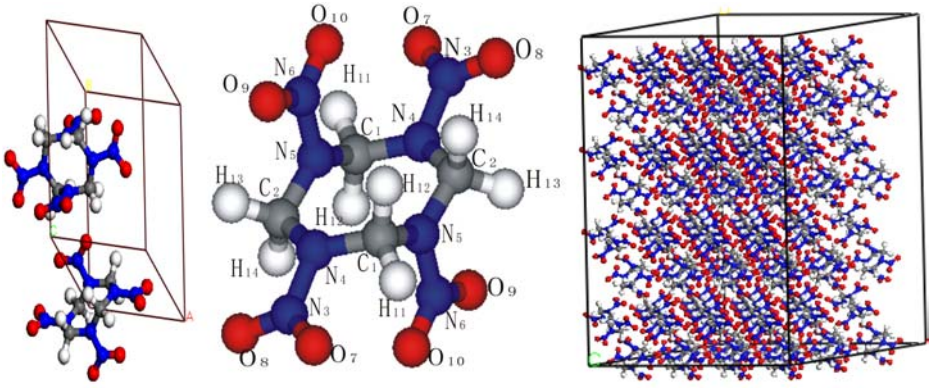

Figure 1. The unit cell of the β-HMX crystal (left) and the conformation of the $C_4H_8N_8O_8$ molecule in β-HMX (middle). The supercell of the β-HMX crystal (right). Grey, blue, red and white spheres represent C, N, O and H atoms, respectively (colour online).

interactions were managed using the atom-based summation method [28].

3. Results and discussion

3.1 DFT calculations

3.1.1 Crystal structure at ambient pressure

The structural parameters such as lattice constants of a molecular crystal are important as a benchmark for the performance of theoretical approach to describe the intermolecular interaction and to evaluate the crystal stability at ambient pressure. Figure 1 displays the unit cell of the crystalline β-HMX and the conformation of the $C_4H_8N_8O_8$ molecule in β-HMX. Here, we tested two approximations of exchange-correlation interaction, namely LDA and GGA/PBE. The theoretical lattice parameters, unit cell volume and crystalline density of bulk β-HMX are given in Table 1, together with the experimental data [7]. From Table 1, it can be seen that the LDA performs better than the GGA. The LDA calculations yield the lattice constants of $a = 6.45$ Å, $b = 10.52$ Å, $c = 8.61$ Å and $\beta = 123.9°$, with discrepancies to experiments by 1.37, 4.79, 1.03 and 0.32%, respectively. The unit cell volume from the LDA calculation is lower than the experimental volume by 6.63%. On the other hand, the GGA overestimates the cell volume of β-HMX by 9.86% and the errors of GGA results with regard to experiments are 3.37, 3.7, 1.84 and 0.4 for a, b, c and β, respectively. The discrepancies between theory and experiment are primarily due to a lack of vdW dispersion force in the conventional DFT functional. The bond lengths and bond angles of β-HMX from the LDA and GGA/PBE calculations are listed in Table 2, together with the experimental data and previous theoretical results. Table 2 also compares the geometry parameters of the β-HMX molecule in the gas phase [29], solid phase [15] and from the experimental data of the ambient solid phase [7]. The average deviations of the computed bond lengths with respect to the experimental data [7] are 0.05% for N—N, 2.21% for O—N, 0.65% for N—C and 1.13% for H—C in the LDA case, and 0.93% for N—N, 2.41% for O—N, 0.58% for N—C and 1.27% for H—C in the GGA case. All computed bond angles agree reasonably with previous theoretical results and experimental values. According to our present results, the LDA is more suitable for describing the structural properties of the β-HMX crystal, thus we shall use it in the rest of this paper.

3.1.2 Electronic structures at ambient pressure

Based on the equilibrium crystal structure of β-HMX from the LDA calculations, we computed the electronic band structures of the β-HMX crystal at ambient conditions, as shown in Figure 2. The band dispersions are almost flat along the Brillouin zone, consistent with the character of the HMX molecules. The electronic gap (ΔE) between the valence and conduction bands is 3.059 and 3.061 eV from the LDA and GGA calculations, respectively, indicating

Table 1. Theoretical lattice parameters of β-HMX compared with the experimental data.

Method	a (Å)	b (Å)	c (Å)	β (°)	α, γ (°)	V (Å^3)	ρ (g/cm^3)
Exp. [7]	6.54	11.05	8.7	124.3	90.0	519.387	1.89369
LDA/CA-PZ	6.45	10.52	8.61	123.9	90.0	484.912	2.02832
GGA/PBE	6.76	11.46	8.86	123.8	90.0	570.372	1.72422

Note: LDA/CA-PZ, LDA of Ceperly and Adler by the parameterisation of Perdew and Zunger.

Table 2. Geometry parameters of the β-HMX crystal: bond lengths A—B (Å) and bond angles A—B—C (°).

	This work		Others			
	LDA	GGA	GGA [15]	LDA [15]	[29]	Exp. [7]
Bond lengths						
N_3—N_4	1.3726	1.3895	1.3924	1.3659	1.3976	1.3735
N_5—N_6	1.3542	1.3637	1.3730	1.3529	1.3923	1.3538
N_3—O_7	1.2419	1.2430	1.2452	1.2435	1.2253	1.2095
N_3—O_8	1.2406	1.2455	1.2424	1.2484	1.2256	1.2046
N_6—O_9	1.2409	1.2456	1.2441	1.2469	1.2236	1.2331
N_6—O_{10}	1.2520	1.2529	1.2534	1.2539	1.2302	1.2209
C_1—N_4	1.4414	1.4444	1.4455	1.4391	1.4608	1.4549
C_1—N_5	1.4461	1.4456	1.4408	1.4316	1.4510	1.4475
C_2—N_4	1.4209	1.4235	1.4268	1.4196	1.4416	1.4368
C_2—N_5	1.4655	1.4648	1.4681	1.4574	1.4774	1.4725
C_1—H_{11}	1.1228	1.0889	1.0922	1.1079	1.0921	1.1104
C_1—H_{12}	1.0952	1.0914	1.0903	1.1045	1.0894	1.0906
C_2—H_{13}	1.1175	1.0896	1.0899	1.1064	1.0884	1.1006
C_2—H_{14}	1.1086	1.0894	1.0934	1.1049	1.0933	1.0942
Bond angles						
C_1—N_4—C_2	123.077	123.185	122.796	123.906	123.59	123.799
N_4—C_2—N_5	110.612	110.099	111.605	110.229	111.30	110.126
C_2—N_5—C_1	123.029	123.791	123.835	123.112	123.21	122.394
N_5—C_1—N_4	112.252	113.352	113.068	111.126	114.23	113.516
C_1—N_4—N_3	117.928	117.156	117.988	118.37	117.89	117.369
C_1—N_5—N_6	118.992	118.976	119.068	119.016	118.16	118.211
C_2—N_4—N_3	117.305	117.183	118.502	117.618	118.10	118.152
C_2—N_5—N_6	115.638	115.593	115.609	116.056	114.44	115.138
O_7—N_3—O_8	126.189	126.557	126.747	126.288	127.37	126.650
O_7—N_3—N_4	116.586	116.204	116.953	116.824	116.73	115.899
O_8—N_3—N_4	116.217	116.095	116.286	116.854	115.88	117.446
O_9—N_6—O_{10}	125.087	125.717	125.768	125.478	126.76	125.906
O_9—N_6—N_5	115.610	115.493	115.553	115.855	115.13	116.206
O_{10}—N_6—N_5	117.016	117.362	118.665	118.652	118.05	117.886
H_{11}—C_1—H_{12}	108.212	107.109	108.414	107.578	109.43	106.183
H_{11}—C_1—N_4	108.005	108.613	106.520	107.300	105.92	106.602
H_{11}—C_1—N_5	110.119	109.863	110.929	111.725	109.81	108.515
H_{12}—C_1—N_4	111.318	111.771	111.428	111.94	111.24	111.834
H_{12}—C_1—N_5	108.570	108.213	106.448	107.166	106.20	109.823
H_{13}—C_2—H_{14}	109.330	109.584	108.554	109.146	108.78	109.671
H_{13}—C_2—N_4	110.845	109.749	109.995	109.800	109.90	110.508
H_{13}—C_2—N_5	109.366	109.957	108.502	109.527	108.53	109.190
H_{14}—C_2—N_4	107.455	108.923	108.379	107.869	108.23	107.253
H_{14}—C_2—N_5	110.577	109.513	109.759	110.244	110.07	110.074

that β-HMX is an insulator. It is well known that DFT methods within either the LDA or GGA usually underestimate the band gap of the materials. Generally speaking, the materials with a larger band gap are expected to be relatively more stable or less sensitive. Compared with the theoretical results of the bicyclo-HMX solid ($\Delta E = 3.44$ eV) [30] and the trans-1,4,5,8-tetranitro-1,4,5,8-tetraazadecalin (TNAD) solid ($\Delta E = 3.3$ eV) [31], β-HMX has a smaller energy gap. Thus, it is concluded that β-HMX is more sensitive or less stable than the bicyclo-HMX and TNAD solid.

To further discuss the bonding nature of the β-HMX crystal, its total electronic density of states (DOSs) and partial DOS (PDOSs) were calculated and are shown in Figure 3. β-HMX exhibits a sharp peak in the upper valence band near the Fermi level, which originates from the p states. In the upper valence band, several main peaks are contributed from the s and p states. The conduction bands mainly come from the p states. This indicates that the p states for β-HMX play a vital role in the chemical reaction. According to Figure 3, we can conjecture the basic properties of β-HMX as follows. In the upper valence band, the PDOS from C atoms is far lower than those of the H, O and N states, suggesting that the H, O and N make more significant contributions to the valence bands than C. In the energy range from −25 to −13 eV, several pronounced peaks associated with the H, O and N atoms are observed. In the conduction band region, the peaks mainly originate from the p states of C, H and N

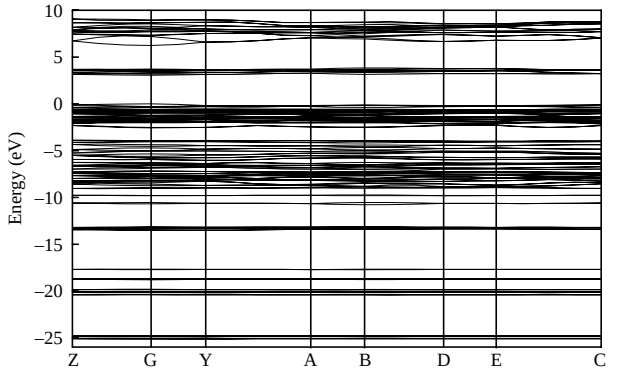

Figure 2. Calculated band structure of β-HMX along different symmetry directions of the Brillouin zone. The Fermi energy level was taken as zero energy.

atoms. In other words, the frontier bands are mainly formed by the p states of C, H and N atoms.

3.1.3 *Crystal structure under hydrostatic pressure*

To examine the effect of hydrostatic compression on the crystal structure, we compared the calculated crystallographic lattice parameters, volume and density for the β-HMX unit cell in the pressure range of 0–40 GPa with zero-pressure experimental data as shown in Figure 4. Figure 4(a) shows the unit cell volume V as a function of pressure for β-HMX. At lower pressures, the discrepancy between our results and other experimental results [7,8,32] is relatively larger. This disagreement is reduced at higher pressures. Due to the restriction of the relaxation method

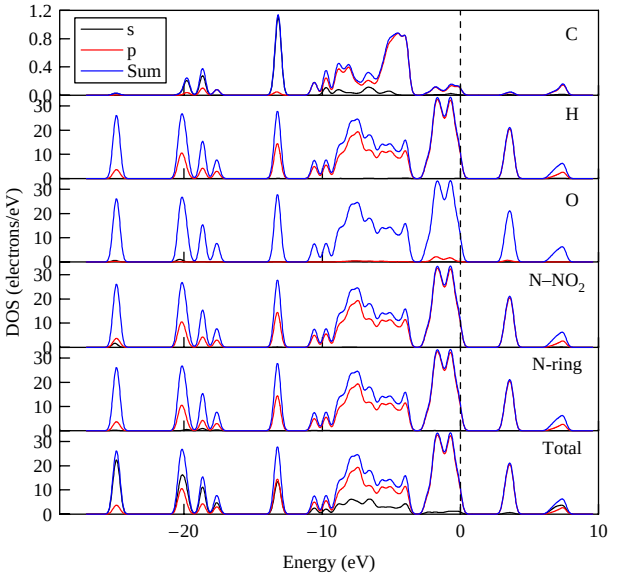

Figure 3. Calculated total DOSs and PDOSs of C, H, O, N in NO_2 and ring of β-HMX at ambient pressure. The Fermi energy is shown as a dashed vertical line.

and simulation supercell, we did not observe a phase transition within the pressure range of 0–40 GPa, while a phase transition occurred at 27 GPa in experiment [7]. With increasing pressure, the lattice dimensions are compressed greatly and the crystalline density of β-HMX increases significantly. Up to a high pressure of 40 GPa, the mass density increases by 55.2% with respect to the zero-pressure value. Generally speaking, the detonation velocity and detonation pressure increase greatly with increasing density and its square [33], respectively. It is very important to increase the density for enhancing the performance of an explosive or a propellant. When the density of a compound is larger than 1.9 g/cm^3, the detonation velocity greater than 9 km/s and detonation pressure over 40 GPa, it can be regarded as a high energy density compound. Hence, one can increase the density of the β-HMX solid above 1.9 g/cm^3 via compression.

It is also noteworthy that the compressibility of β-HMX is anisotropic. A large compression occurs along the b-axis than along the a- and c-axes. The pressure dependence of the lattice constants is shown in Figure 4(b), where our theoretical results are compared with experimental data given by Yoo and Cynn [7] and previous simulation results givne by Lu et al. [15]. We find that the β-HMX crystal is much stiffer along the b direction (change in the lattice constant is 4.4% from 0 to 40 GPa) than along the a (lattice change by 11.9% up to 40 GPa) and c (lattice change by 23.6% up to 40 GPa) directions. This means that the intermolecular interactions along the three crystallographic directions increase in the order of $b < a < c$. Such anisotropic behaviour can be understood in terms of the anisotropic intermolecular interaction in this crystal. In other words, the β-HMX solid shows an anisotropic compressibility. Within the entire pressure range studied, the cell angles α and γ remain unchanged, while the angle β shows slight oscillations with pressure.

3.1.4 *Electronic structure under hydrostatic pressure*

Within the pressure range of 0–40 GPa, we examined the effect of hydrostatic pressure on the electronic structure of β-HMX by calculating the band structure and DOS, which are shown for several selected pressures in Figures 5 and 6, respectively. We found that both band structures and DOS are insensitive to pressure. The band gap of the β-HMX crystal reduces from 3.059 to 2.890 eV as the pressure increases from 0 to 2.5 GPa. When the pressure further increases from 5 to 40 GPa, the band gap decreases slowly from 2.786 to 2.436 eV. Moreover, there is a significant increase in the bandwidth of different groups from 0 to 2.5 GPa and only a slight increase from 2.5 to 40 GPa. This shows that the probability of electron transitions from the occupied valence bands to the empty conduction bands increases under compression. A similar behaviour was observed from the DOS analysis in Figure 6.

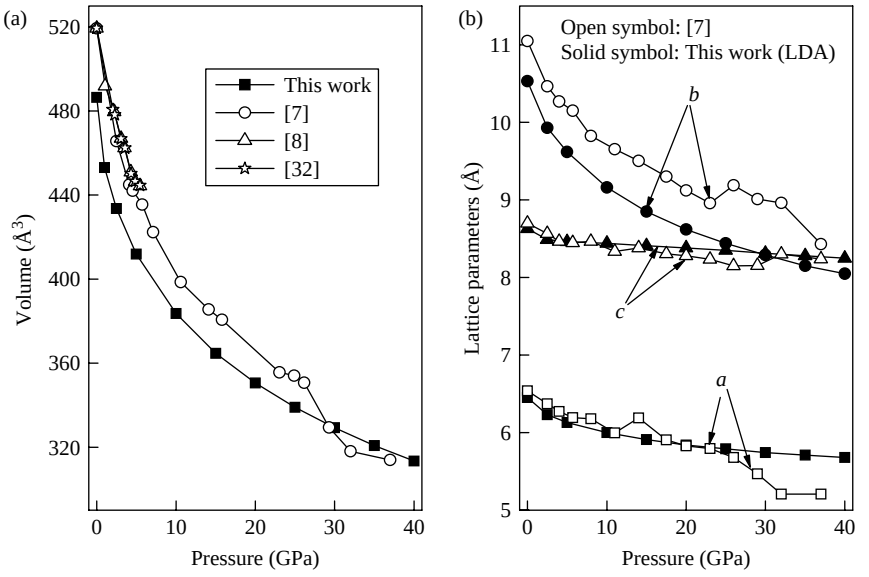

Figure 4. (a) The unit cell volume V as a function of pressure for β-HMX and (b) pressure dependence of the lattice constants for β-HMX.

The characteristic peaks in the DOS become slightly more dispersed with further increment of pressure from 10 GPa, corresponding to the enhanced electronic delocalisation in β-HMX under hydrostatic pressures. All electronic states gradually shift towards the negative energy region. These theoretical results have some implications on the detonation sensitivity and stability of β-HMX under high pressure. With increasing pressure from 0 to 40 GPa, the impact sensitivity of β-HMX would increase gradually.

3.2 MD simulations

3.2.1 Choice of force field and equilibrium of system

In order to choose a suitable force field, we carried out a series of tests for the β-HMX crystal. The parameters of the COMPASS force field have been tested and confirmed by comparing with the first-principles calculations and the experimental values. The non-bond parameters have been further modified by the thermal–physical properties of liquid and solid molecules obtained from the MD method. In previous studies, the COMPASS force field was employed in the MD simulations of many nitramine explosives, such as bicycle-HMX [30], CL-20 [34] and TNAD [31,35]. As shown in Table 3, the theoretical results of lattice parameters and atomic fractional coordinates are in good agreement with the experiment, indicating that the COMPASS force field is appropriate for simulating the β-HMX crystal.

Before the statistic analysis, the system must reach the equilibrium state. The equilibrium of the system is achieved when the fluctuations of the temperature and energy are less than 5–10%. Typically, the system should achieve its equilibrium in the initial 100 ps, and followed by a production run of last 1×10^5 time steps. As a representative, Figure 7 shows the equilibrium curves of the temperature and energy in the MD simulation of β-HMX at 298 K for the last 5×10^4 steps during the equilibration runs. It can be seen that the system temperature has reached its equilibrium state within 298 ± 11 K. The amplitudes of fluctuations for the potential energy and non-bond energy are less than 0.3 and 0.2%, respectively, showing that the system has reached its energy equilibrium. After equilibrium, production runs of 100 ps were then performed.

3.2.2 Crystal structure

Within NPT ensembles, we simulated the structural properties of β-HMX at 0 GPa and in the temperature range from 5 to 400 K. The lattice parameters and cell volumes vary nonlinearly with temperature and exhibit abrupt changes at 360 K. With temperature increasing from 5 to 360 K, the lattice parameters and cell volumes increase and the crystalline density of β-HMX decreases gradually. In the temperature range of 5–350 K, changes in lattice parameters vary from −0.917 to 1.376%, −0.905 to 1.448% and −0.916 to 1.494% for a, b and c, respectively; the cell volume changes from −2.783 to 4.361%. The results are displayed in Figure 8, which shows that the β-HMX crystal undergoes a phase transition at 360 K, in agreement with the experimental observation of the phase transition at 375–377 K [3]. Within the entire temperature range considered, the lattice angles remain almost invariant, i.e. α and γ are

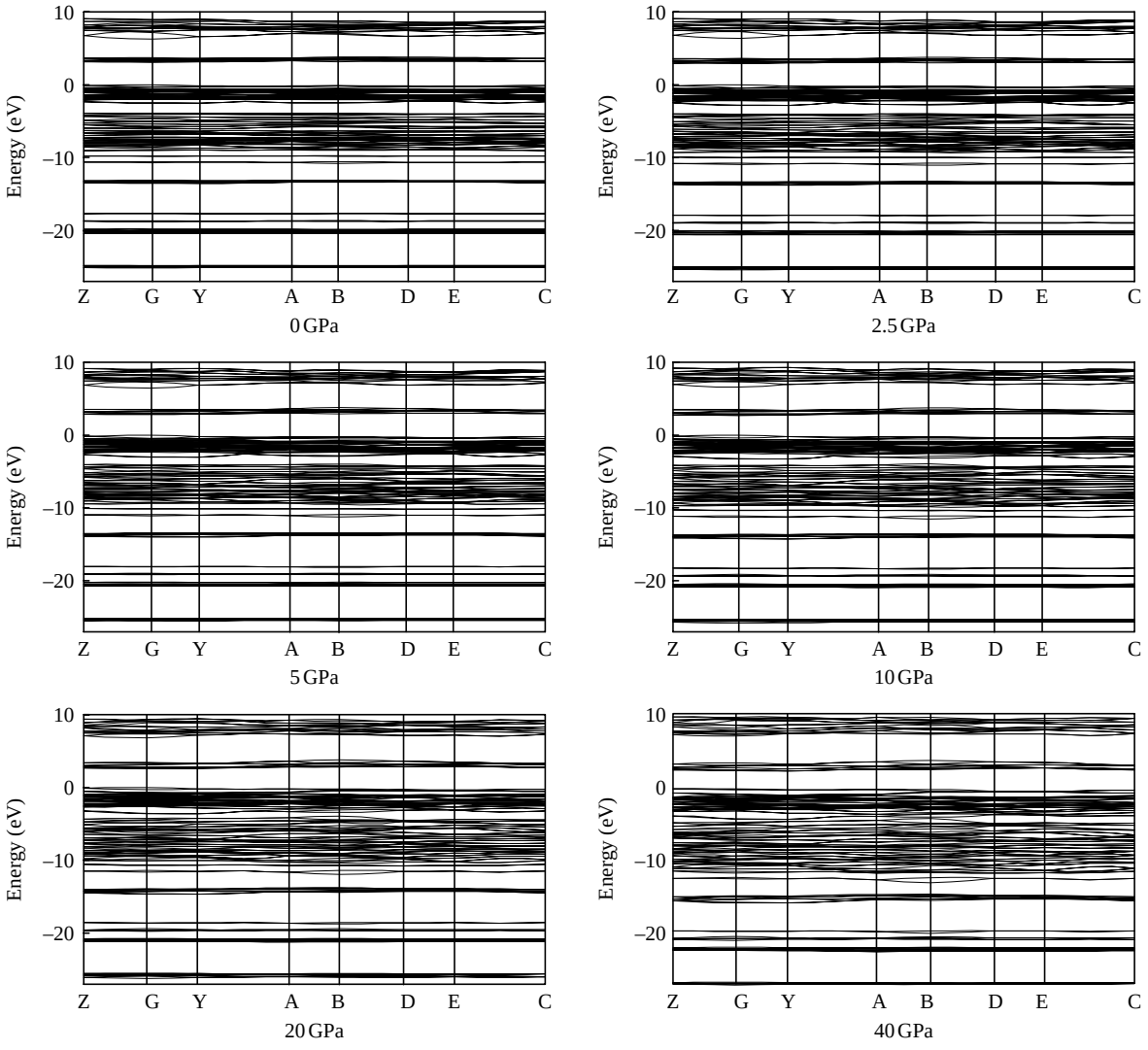

Figure 5. Calculated band structures of β-HMX under different hydrostatic pressures.

approximately equal to 90° and β remains approximately 124.3°.

The thermal expansion coefficient is an important parameter to characterise not only the physical but also the explosive behaviour of energetic materials. In practice, the thermal expansion coefficient can affect the manufacture, storage and transportation of energetic materials. The linear thermal expansion coefficients along the *a*-, *b*-, *c*-axes and volume coefficients of the β-HMX solid at 298 K from our MD simulations are 5.134×10^{-5}, 5.133×10^{-5}, 5.038×10^{-5} and 1.492×10^{-4}/K, respectively. The linear coefficients of β-HMX agree with the previous experimental result of 5.04×10^{-5}/K [36]. Figure 8 shows that the thermal expansion of the β-HMX crystal is weakly anisotropic. Expansions along the crystal axes *b* and *c* are 2.37 and 2.44%, respectively; both are slightly larger than that along the *a*-axis (2.31%) in the temperature range of 5–350 K. Furthermore, we found that both the linear and volume thermal expansions of β-HMX vary slightly with the temperature increasing from 5 to 350 K, but the temperature effect on the thermal expansion can be nearly ignored due to the very small amplitude. The thermal expansion is associated with other important thermodynamic properties such as the Grüneisen parameter and Rayleigh number. We expect that this study can be useful for the investigation of these properties.

3.2.3 Mechanical properties

On the basis of NPT-MD simulation trajectories, each structure is subjected to uniaxial tensile and pure shear deformations, and the induced stress tensors can be obtained from the virial formalism in atomistic calculations. The elastic coefficients can be obtained by taking the first derivatives of the stress with respect to strain [37].

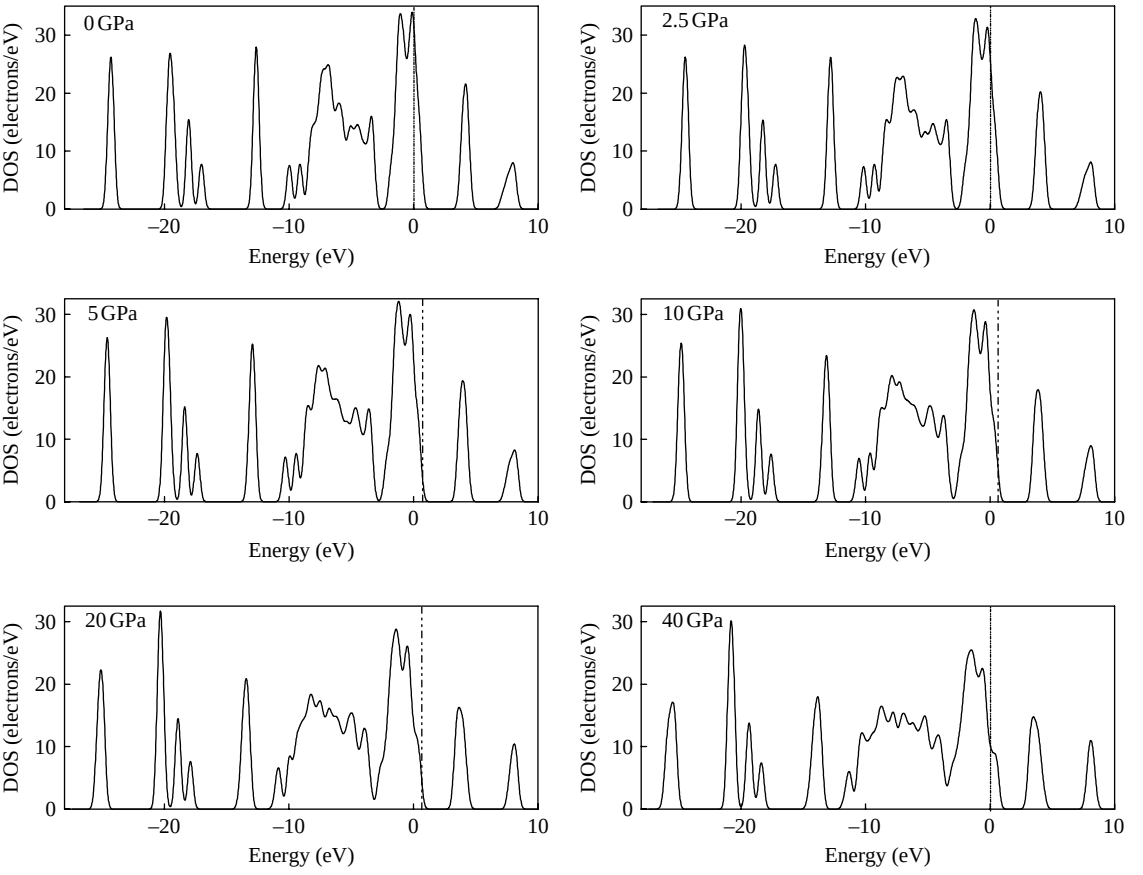

Figure 6. Calculated total DOS of β-HMX under different hydrostatic pressures.

For β-HMX, there are 13 independent elastic coefficients. Afterwards, we can estimate the Young modulus and the Poisson ratio from the least-squares fits of the average tensile stress vs. tensile strain, respectively. We can also compute other mechanical parameters, such as the bulk modulus, shear modulus and Lamé coefficients. Here, the second-order elastic tensors and various elastic moduli, including the Young modulus (E), bulk modulus (K) and shear modulus (G) and the Poisson ratio (γ), of the β-HMX crystal have been evaluated at ambient pressure in the temperature range of 5–400 K using the isothermal–isobaric simulation trajectories and the elastic–static method. The results together with other theoretical and experimental values are presented in Tables 4 and 5, respectively.

From Table 4, it can be found that there is remarkable anisotropy in the diagonal elements C_{ii} ($i = 1$–6) of the elastic constant tensor, which can be related to the crystal structure. Generally speaking, the diagonal elements C_{ii} describe the crystal stiffness under uniaxial compression and shear, while the off-diagonal elements C_{ij} ($i \neq j$) correspond to biaxial compression and distortion of the crystal. Therefore, it can be concluded that the β-HMX material is anisotropic upon compression and has a good stability to shear deformation perpendicular to the c-axis. Most of the elastic constants decrease with increasing temperature from 5 to 360 K. The reduction for the constants C_{11}, C_{22}, C_{33} and the off-diagonal elements C_{12}, C_{13}, C_{23} are especially remarkable, whereas those for the shear constants C_{55} and C_{66} are less pronounced. On the contrary, C_{15}, C_{25}, C_{35} and C_{46} increase with increasing temperature. This result suggests that the overall crystal rigidity decreases and the anisotropy is enhanced slightly with increasing temperature.

It is known that the Cauchy pressure ($C_{12}-C_{44}$) can be used as a standard to estimate the ductility or brittleness of a material [38]. The ($C_{12}-C_{44}$) value of a ductile material is positive, whereas the negative value corresponds to a brittle material. The larger the positive ($C_{12}-C_{44}$) value of a material, the more ductile is this material. The ($C_{12}-C_{44}$) data given in Table 4 indicate that β-HMX is a brittle material with the negative ($C_{12}-C_{44}$) value. Our results agree with other theoretical [11,39] and experimental [9,40,41] results within the similar temperature range.

Table 5 lists the effective isotropic mechanical properties of β-HMX under different temperatures, including the Young modulus E, bulk modulus K, shear modulus G, the Poisson ratio γ, Lamé coefficients λ and μ,

Table 3. Lattice parameters and atomic coordinates simulated by the COMPASS force field compared with experimental values of β-HMX.

	a (Å)	b (Å)	c (Å)	β (°)	α, γ (°)	V (Å^3)	ρ (g/cm^3)
Exp. [7]	6.54	11.05	8.70	124.3	90.0	519.387	1.89369
MD	6.58	11.12	8.76	124.3	90.0	529.827	1.85638

	COMPASS			Exp. [7]		
Atom	u	v	w	u	v	w
C_1	−0.1922	0.0648	−0.2198	−0.1976	0.0656	−0.2183
C_2	−0.2509	−0.1169	−0.0488	−0.2442	−0.1144	−0.5530
C_3	0.1922	0.5648	0.7198	0.1976	0.5656	0.7183
C_4	0.2509	0.3832	0.5488	0.2442	0.3856	0.5553
H_1	−0.3172	0.1343	−0.3311	−0.3274	0.1385	−0.3195
H_2	−0.0838	0.0134	−0.2653	−0.0923	0.0235	−0.2739
H_3	−0.3407	−0.2114	−0.1085	−0.3299	0.2066	−0.1165
H_4	−0.2903	−0.0866	0.0554	−0.2911	0.0858	−0.0473
H_5	0.3171	0.6343	0.8311	0.3274	0.6385	0.8191
H_6	0.0838	0.5134	0.7653	0.0923	0.5235	0.7739
H_7	0.3407	0.2886	0.6085	0.3299	0.2934	0.6165
H_8	0.2903	0.4134	0.4446	0.2911	0.4142	0.4527
O_1	−0.6941	0.0783	−0.4301	−0.6956	0.0719	−0.4192
O_2	−0.7147	−0.0557	−0.2372	−0.7036	−0.0606	−0.2403
O_3	0.0543	0.2546	0.1878	0.0475	0.2464	0.1816
O_4	−0.3337	0.2302	−0.0655	−0.3308	0.2197	−0.0650
O_5	0.6941	0.5783	0.9301	0.6956	0.5719	0.9192
O_6	0.7147	0.4443	0.7372	0.7036	0.4394	0.7403
O_7	−0.0543	0.7546	0.3122	−0.0475	0.7464	0.3184
O_8	0.3337	0.7302	0.5655	0.3308	0.7197	0.5650
N_1	−0.5983	0.0028	−0.2939	−0.5945	−0.0006	−0.2919
N_2	−0.3491	−0.0217	−0.1990	−0.3407	−0.2600	−0.2030
N_3	−0.0138	0.1281	−0.0453	−0.0185	0.1211	−0.0376
N_4	−0.1024	0.2101	0.0294	−0.1081	0.2021	0.3004
N_5	0.5983	0.5028	0.7939	0.5945	0.4994	0.7919
N_6	0.3491	0.4783	0.6990	0.3407	0.4740	0.7030
N_7	0.0138	0.6281	0.5453	0.0185	0.6211	0.5376
N_8	0.1024	0.7101	0.4706	0.1081	0.7021	0.4696

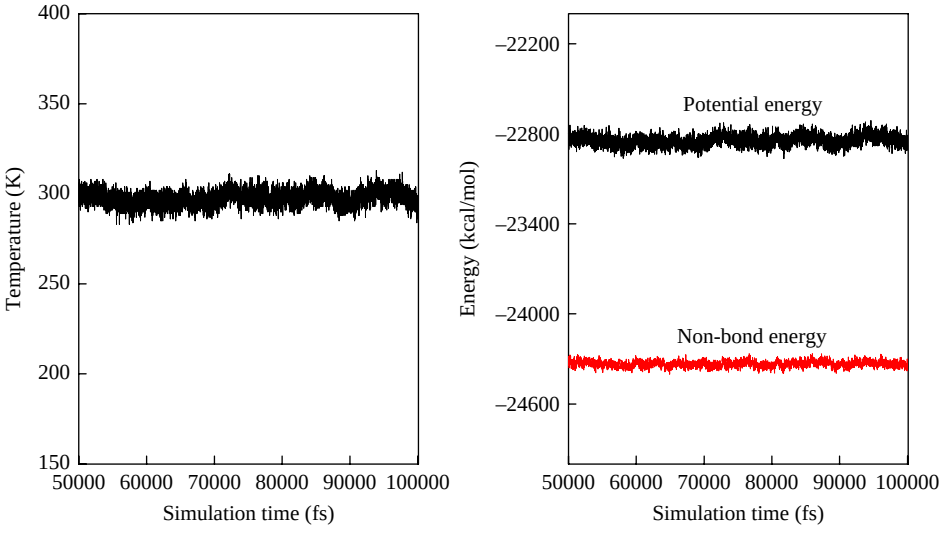

Figure 7. Fluctuation curves of the temperature and energy in the last 5×10^4 simulation steps of the NPT-MD equilibration run for β-HMX at 298 K.

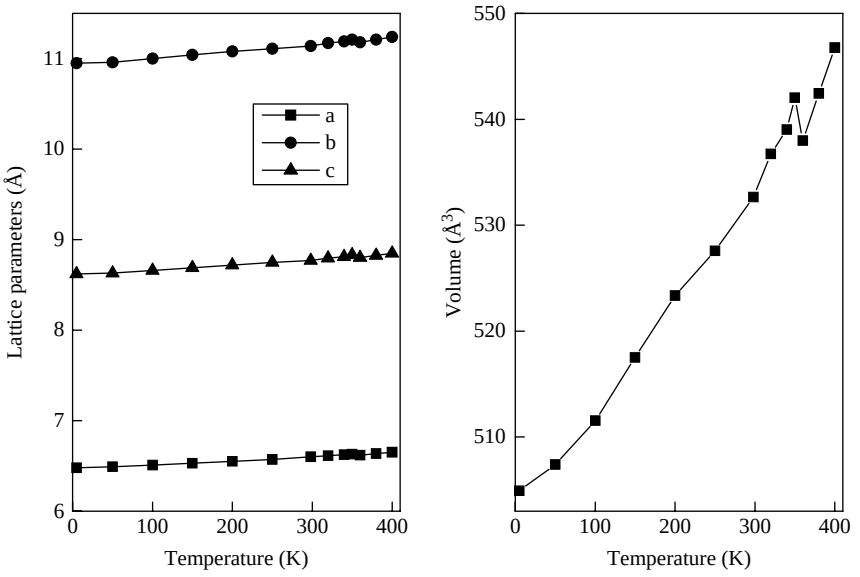

Figure 8. Lattice constants and unit cell volume V as a function of temperature for β-HMX; V_0 denotes the volume at 0 K and 0 GPa of β-HMX.

and *K/G* ratio. It can be seen that, at low temperature, β-HMX has larger stiffness, plasticity and fracture strength to resist the external stress. With increasing temperature, all the isotropic moduli decrease gradually, thus the rigidity and brittleness of β-HMX decrease. This indicates that β-HMX will deform more easily when it is subjected to an external loading at a higher temperature. Such a result can be understood in the light of the following two assumptions: (1) the internal free volume expands more severely with the increase of temperature and (2) the molecules within the crystal gain more kinetic energy when the temperature rises. It is interesting to note that the reduction in shear modulus is smaller than that in the Young modulus and bulk modulus in the temperature region from 5 to 360 K. This is consistent with the less changes in the shear constants C_{55} and C_{66} with increasing temperature. Hence, we suggested that β-HMX possesses good stability to shear loading in the temperature range of 5–360 K. The Poisson ratio can also be used as a standard to estimate the plasticity of a material. From our MD

Table 4. Theoretical elastic constants (GPa) of β-HMX with zero pressure and different temperatures compared with other results.

T (K)	C_{11}	C_{22}	C_{33}	C_{44}	C_{55}	C_{66}	C_{12}	C_{13}	C_{15}	C_{23}	C_{25}	C_{35}	C_{46}	$C_{12}-C_{44}$
5	22.5	16.4	20.5	9.04	5.15	6.68	6.50	8.47	−0.74	10.7	−4.17	−1.94	−3.32	−2.54
50	21.2	15.4	19.5	8.69	5.00	6.41	6.07	7.89	−0.68	9.89	−3.96	−1.81	−3.15	−2.62
100	19.7	14.2	18.2	8.25	4.81	6.07	5.57	7.22	−0.59	8.90	−3.72	−1.64	−2.94	−2.68
150	18.1	13.0	16.9	7.79	4.63	5.74	5.09	6.54	−0.50	7.90	−3.46	−1.48	−2.73	−2.70
200	16.5	11.7	15.5	7.31	4.42	5.36	4.59	5.85	−0.38	6.85	−3.20	−1.30	−2.51	−2.72
250	15.0	10.6	14.3	6.85	4.23	5.01	4.16	5.23	−0.26	5.93	−2.95	−1.12	−2.30	−2.69
298	13.6	9.50	13.2	6.41	4.04	4.68	3.75	4.66	−0.15	5.07	−2.71	−0.96	−2.10	−2.66
320	13.1	9.18	12.8	6.26	3.99	4.56	3.62	4.48	−0.11	4.80	−2.63	−0.90	−2.04	−2.64
340	12.5	8.71	12.3	6.06	3.90	4.40	3.43	4.24	−0.06	4.43	−2.52	−0.82	−1.95	−2.63
350	12.0	8.30	11.8	5.87	3.82	4.27	3.28	4.01	−0.01	4.11	−2.43	−0.75	−1.88	−2.59
360	11.9	8.23	11.7	5.84	3.80	4.24	3.25	3.98	−0.009	4.05	−2.41	−0.74	−1.86	−2.59
380	11.4	7.88	11.4	5.68	3.74	4.12	3.11	3.79	0.04	3.78	−2.33	−0.68	−1.80	−2.57
400	10.9	7.50	11.0	5.50	3.66	3.99	2.96	3.59	0.08	3.48	−2.24	−0.60	−1.73	−2.54
[9]	18.4	14.4	12.4	4.8	4.8	4.5	6.4	10.5	−1.1	6.4	0.8	1.1	2.8	1.6
[11]	22.2	23.9	23.4	9.2	11.1	10.0	9.6	13.2	−0.1	13.0	4.7	1.6	2.5	0.4
[39]	12.8	10.9	11.4	5.9	4.6	4.8	3.4	4.9	−0.4	5.2	−2.7	−0.4	−1.8	−2.5
[40]	19.4	17.5	17.8	9.1	9.2	9.8	5.9	8.4	−1.1	8.2	0.83	0.2	2.4	−3.2
[41]	20.8	26.9	18.5	4.2	6.1	2.5	4.8	12.5	−0.5	5.8	−1.9	1.9	2.9	0.6

Notes: Values determined by Brillouin scattering at 293 K and 1 atm [9] (experimental results). Values determined by MD simulation at 295 K and 1 atm [11] (theoretical results). Values determined by MD simulation at 295 K under atmospheric pressure [39] (theoretical results). Results determined by Sewell et al. [40] (experimental results). Values determined by Zaug [41] (experimental results).

Table 5. Mechanical properties of the β-HMX crystal under different temperatures.

T (K)	Young's modulus, *E* (GPa)	Bulk modulus, *K* (GPa)	Shear modulus, *G* (GPa)	Poisson's ratio, γ	Lamé coefficient, λ	Lamé coefficient, μ	*K*/*G*
5	14.65	12.30	5.626	0.3016	8.553	5.626	2.186
50	13.96	11.53	5.375	0.2983	7.950	5.375	2.145
100	13.11	10.61	5.066	0.2940	7.228	5.066	2.094
150	12.23	9.672	4.745	0.2892	6.509	4.475	2.038
200	11.30	8.696	4.403	0.2834	5.761	4.403	1.975
250	10.45	7.834	4.091	0.2776	5.107	4.091	1.915
298	9.646	7.021	3.794	0.2710	4.492	3.794	1.851
320	9.388	6.768	3.699	0.2688	4.302	3.699	1.830
340	9.025	6.412	3.566	0.2654	4.035	3.566	1.798
350	8.706	6.099	3.449	0.2621	3.800	3.449	1.768
360	8.649	6.043	3.428	0.2614	3.757	3.428	1.763
380	8.379	5.778	3.330	0.2583	3.558	3.330	1.735
400	8.081	5.492	3.220	0.2547	3.345	3.220	1.706
[9]		9.6	3.1				3.097
[11]		15.1	7.0				2.157
[39]	9.2	6.9	3.6	0.3			1.917
[41]		12.5	1.3				9.615

Notes: Values determined by Brillouin scattering at 293 K and 1 atm [9] (experimental results). Values determined by MD simulation at 295 K and 1 atm [11] (theoretical results). Values determined by MD simulation at 295 K under atmospheric pressure [39] (theoretical results). Values determined by Zaug [41] (experimental results).

simulation, the Poisson ratio decreases from 0.3016 to 0.2614 as the temperature rises from 5 to 360 K. This suggests that β-HMX exhibits plasticity in the range of 5–360 K. On the other hand, the extent of the plastic range for a material can be evaluated by the ratio of the bulk modulus to shear modulus, i.e. *K*/*G* [42]. A higher *K*/*G* value denotes more malleability and a lower value means brittleness [42]. In Table 5, it can be deduced that β-HMX has better malleability at lower temperature, in agreement with the conclusion drawn from the Cauchy pressure ($C_{12}-C_{14}$).

4. Conclusions

In this paper, periodic DFT calculations and classic MD simulations are performed to study the structural, electronic and mechanical properties of the energetic material β-HMX. The effects of hydrostatic pressure and temperature on the structures and physical properties are discussed. The crystal structure of β-HMX from both LDA calculations and COMPASS force-field simulations compares reasonably with experiments. The computed band structures and DOS show that the β-HMX crystal at zero-pressure has a band gap of 3.059 eV. Under hydrostatic pressures, the compressibility of β-HMX is anisotropic with the largest compression along the *b*-axis. With increasing external pressure, β-HMX crystal gradually changes from insulator towards metallic, which is demonstrated by the reduction in band gap. As temperature increases from 5 to 400 K, the lattice parameters show nonlinear dependence on the temperature. An interrupt of the volume at 360 K was observed, which indicates the occurrence of a phase transition in β-HMX. Thermal expansion of β-HMX is anisotropic with slightly larger expansion coefficients along the *b*- and *c*-axes than along the *a*-axis. The computed elastic tensors show considerable anisotropy of the β-HMX solid. Within a temperature range of 5–360 K, β-HMX possesses a good plasticity and its stiffness decreases with increasing temperature. We expect that these theoretical results will be helpful for understanding the behaviour of β-HMX at high temperatures and/or high pressures.

Acknowledgements

This work was supported by the National Key Laboratory Fund for Shock Wave and Detonation Physics Research of the China Academy of Engineering Physics under Grant No. 9140C6711010805, the National Science Foundation of China under the Contract No. 20773085 and the State Key Laboratory of Explosion Science and Technology, Beijing Institute of Technology under Grant Nos. KFJJ08-5 and KFJJ09-02, as well as Rui-Feng Co. and the Virtual Laboratory for Computational Chemistry of CNIC, and the Supercomputing Center of CNIC, Chinese Academy of Science.

References

[1] P.W. Cooper and S.R. Kurowski, *Introduction to the Technology of Explosives*, Wiley, New York, 1996.
[2] J. Akhaven, *The Chemistry of Explosives*, Royal Society of Chemistry, Cambridge, 1998.
[3] H.H. Cady and L.C. Smith, *Studies on the Polymorphs of HMX*, Los Alamos Scientific Laboratory Report, LAMS-2652 TID-4500; Los Alamos National Laboratory, Los Alamos, NM, 1961.
[4] P. Main, R.E. Cobbledick, and R.W.H. Small, *Structure of the fourth form of 1,3,5,7-tetraazacyclooctane (γ-HMX), $2C_4H_8N_8O_8 \cdot 0.5H_2O$*, Acta Crystallogr. C 41 (1985), pp. 1351–1354.
[5] H.H. Cady, A.C. Larson, and D.T. Cromer, *The crystal structure of α-HMX and a refinement of the structure of β-HMX*, Acta Crystallogr. 16 (1963), pp. 617–623.

[6] C.S. Choi and H.P. Boutin, *Study of the crystal structure of β-cyclotetra-methylene-tetranitramine by neutron diffraction*, Acta Crystallogr. B 26 (1970), pp. 1235–1240.
[7] C.S. Yoo and H. Cynn, *Equation of state, phase transition, decomposition of β-HMX (octahydro-1,3,5,7-tetranitro-1,3,5,7-tetrazocine) at high pressures*, J. Chem. Phys. 111 (1999), pp. 10229–10335.
[8] J.C. Gump and S.M. Peiris, *Isothermal equations of state of beta octahydro-1,3,5,7-tetranitro-1,3,5,7-tetrazocine at high temperatures*, J. Appl. Phys. 97 (2005), 053513–053519.
[9] L.L. Stevens and C.J. Eckhardt, *The elastic constants and related properties of β-HMX determined by Brillouin scattering*, J. Chem. Phys. 122 (2005), 174701.
[10] T.D. Sewell, J. Appl. Phys. 83 (1998), p. 4142.
[11] T.D. Sewell, R. Menikoff, and D. Bedrov, *A molecular dynamics simulation study of elastic properties of HMX*, J. Chem. Phys. 119 (2003), p. 7417.
[12] J.P. Lewis, T.D. Sewell, R.B. Evans, and G.A. Voth, *Electronic structure calculation of the structures and energies of the three pure polymorphic forms of crystalline HMX*, J. Phys. Chem. B 104 (2000), pp. 1009–1013.
[13] E.F.C. Byrd and B.M. Rice, Ab initio *study of compressed 1,3,5,7-tetranitro-1,3,5,7-tetraazacyclooctane (HMX), cyclotrimethylene-trinitramine (RDX), 2,4,6,8,10,12-hexanitrohexaazaisowurzitane (CL-20), 2,4,6-trinitro-1,3,5-benzenetriamine (TATB) and pentaerythritol tetranitrate (PETN)*, J. Phys. Chem. C 111 (2007), pp. 2787–2796.
[14] W.H. Zhu, J.J. Xiao, G.F. Ji, F. Zhao, and H.M. Xiao, *First-principles study of the four polymorphs of crystalline octahydro-1,3,5,7-tetranitro-1,3,5,7-tetrazocine*, J. Phys. Chem. B 111 (2007), pp. 12715–12722.
[15] L.Y. Lu, D.Q. Wei, X.R. Chen, G.F. Ji, Q.M. Zhang, and Z.Z. Gong, *The structural properties of solid β-HMX under compression by the first principle study.* Mol. Phys. 106 (2008), pp. 2569–2580; L.Y. Lu, D.Q. Wei, X.R. Chen, G.F. Ji, X.J. Wang, J. Chang, Q.M. Zhang, and Z.Z. Gong, *The pressure induced phase transition of the solid β-HMX*, Mol. Phys. 107 (2009), pp. 2373–2385.
[16] F.J. Zerilli and M.M. Kuklja, Shock Compression of Condensed Matter. CP955 (2007), pp. 437–440.
[17] M.C. Payne, M.P. Teter, D.C. Allan, T.A. Arias, and J.D. Joannopoulos, *Iterative minimization techniques for* ab initio *total-energy calculations: molecular dynamics and conjugate gradients*, Rev. Mod. Phys. 64 (1992), pp. 1045–1097.
[18] D. Vanderbilt, *Soft self-consistent pseudopotentials in a generalized eigenvalue formalism*, Phys. Rev. B 41 (1990), pp. 7892–7895.
[19] G. Kresse and J. Furthmuller, *Efficient iterative schemes for* ab initio *total-energy calculations using a plane-wave basis set*, Phys. Rev. B 54 (1996), pp. 11169–11185.
[20] T.H. Fischer and J. Almlof, *General methods for geometry and wave function optimization*, J. Phys. Chem. 96 (1992), pp. 9768–9774.
[21] J.P. Perdew, K. Burke, and M. Ernzerhof, *Generalized gradient approximation made simple*, Phys. Rev. Lett. 77 (1996), pp. 3865–3868.
[22] V. Milman, B. Winkler, J.A. White, C.J. Packard, M.C. Payne, E.V. Akhmatskaya, and R.H. Nobes, *Electronic structure, properties and phase stability of inorganic crystals: A pseudopotential plane-wave study*, Int. J. Quantum Chem. 77 (2000), pp. 895–910.
[23] H.J. Monkhorst and J.D. Pack, *Special points for Brillouin-zone integrations*, Phys. Rev. B 13 (1976), pp. 5188–5192.
[24] Accelrys Inc., *Materials Studio*, Accelrys Inc., San Diego, CA, 2004.
[25] H. Sun, *An* ab initio *force-field optimized for condensed-phase*, J. Phys. Chem. B 102 (1998), pp. 7338–7364.
[26] H.J.C. Berendsen, J.P.M. Postma, W.F. Van Gunsteren, A. DiNola, and J.R. Haak, *Molecular-dynamics with coupling to an external bath*, J. Chem. Phys. 81 (1984), pp. 3684–3690.
[27] H.C. Andersen, *Molecular dynamics simulations at constant pressure and/or temperature*, J. Chem. Phys. 72 (1980), pp. 2384–2394.
[28] M.P. Allen and D.J. Tindesley, *Computer Simulation of Liquids*, Oxford University Press, New York, 1989.
[29] H.V. Brand, R.L. Rabie, D.J. Funk, I. Diaz-Acosta, P. Pulay, and T.K. Lippert, *Theoretical and experimental study of the vibrational spectra of the α, β and δ phases of octahydro-1,3,5,7-tetranitro-1,3,5,7-tetrazocine (XMX)*, J. Phys. Chem. B 106 (2002), pp. 10594–11064.
[30] L. Qiu, W.H. Zhu, J.J. Xiao, and H.M. Xiao, *Theoretical studies of solid bicyclo-HMX: Effects of hydrostatic pressure and temperature*, J. Phys. Chem. B 112 (2008), pp. 3882–3893.
[31] L. Qiu, H.M. Xiao, W.H. Zhu, J.J. Xiao, and W. Zhu, Ab initio *and molecular dynamics study of crystalline TNAD (trans-1,4,5,8-tetranitro-1,4,5,8-tetraazadecalin)*, J. Phys. Chem. B 110 (2006), pp. 10651–10661.
[32] B. Olinger, B. Roof, and H. Cady, *Symposium International Sur Le Comportement Des Milieux Denses Sous Hautes Pressions Dynamiques*, Paris, 1978, p. 3.
[33] M.J. Kamlet and S.J. Jacobs, *Chemistry of detonations. I. A simple method for calculating detonation properties of CHNO Explosives*, J. Chem. Phys. 48 (1968), pp. 23–30.
[34] X.J. Xu, H.M. Xiao, J.J. Xiao, W. Zhu, H. Huang, and J.S. Li, *Molecular dynamics simulations of pure ε-CL-20 and ε-CL-20-based PBXs*, J. Phys. Chem. B 110 (2006), pp. 7203–7204.
[35] L. Qiu, W.H. Zhu, J.J. Xiao, W. Zhu, H.M. Xiao, H. Huang, and J.S. Li, *Molecular dynamics simulations of trans-1,4,5,8-tetranitro-1,4,5,8–tetraazadecalin-based polymer-bonded explosives*, J. Phys. Chem. B 111 (2007), pp. 1559–1566.
[36] H.S. Dong and F.F. Zhou, *The Properties of High Explosives and Their Relatives*, Science Press, China, 1989.
[37] J.H. Weiner, *Statistical Mechanics of Elasticity*, Sec. 6.10, Wiley, New York, 1983.
[38] D. Pettifor, *Theoretical predictions of structure and related properties of intermetallics*, Mater. Sci. Technol. 8 (1992), pp. 345–349.
[39] J.J. Xiao, G.Y. Fang, G.F. Ji, and H.M. Xiao, *Simulation investigations in the binding energy and mechanical properties of XMX-based polymer-bounded explosives*, Chin. Sci. Bull. 50 (2005), pp. 21–26.
[40] T.D. Sewell, D. Bedrov, R. Menikoff, and G.D. Smith, *Shock Compression of Condensed Matter*, AIP Conf. Proc. No. 620, Part 1, New York, 2002, p. 399.
[41] J.M. Zaug, *Proceedings of the Eleventh Detonation Symposium*, Snowmass, CO, 1998, p. 498.
[42] S.F. Pugh, *Relations between the elastic moduli and the plastic properties of polycrystalline pure metals*, Philos. Mag. 45 (1954), pp. 823–843.